

CSE 546: MACHINE LEARNING HOMEWORK 3

DAVID P. FLEMING

CONTENTS

Introduction	2
Question 0: Collaborators	2
Question 1: PCA and reconstruction	3
1.0: Details of my PCA implementation	3
1.1: Matrix Algebra Review	3
1.2: PCA	5
1.3: Visualization of the Eigen-Directions	7
1.4: Visualization and Reconstruction	8
2: Let's get to state of the art of MNIST!	14
2.1 Least Squares	15
2.2: EXTRA CREDIT: Softmax Classification	18
2.3: EXTRA CREDIT: Back to those random Neural Net Features	21
3: SVMs: Hinge loss and mistake bounds	24
3.1	24
3.2	24
3.3	24
4: Fitting an SVM classifier by hand	25
4.1	25
4.2	25
4.3	25
4.4	26
4.5	26
5: K-Means	27
5.0: K-Means Algorithm Implementation	27
5.1: Run the algorithm	28
5.2: Classification with K-means	34

Date: November 21st, 2016.

INTRODUCTION

Please note that a copy of all the code I wrote to answer the questions in this assignment are included in my submission but also located online at https://github.com/dflemin3/CSE_546/tree/master/HW3. Some scripts require data, such as MNIST data, to run to completion and were not included on my github due to file size constraints. The MNIST data is included in the `Data` directory as python `.pkl` files as this compressed format gave me quicker load times for my scripts.

Overall, my code is structured as follows: There are three main directories included in my submission: `DML`, `Data` and `HW3`. `HW3` contains all the scripts used to run my analysis. For example to reproduce the answer for Question 1.2, one would run `python hw3_1.2.py`. All scripts have relative file paths so the code should run and have detailed comments to describe functionality. In addition, the scripts have flags near the top to control functionality. By default, I set all flags to true so the script performs the entire analysis and plotting. The `Data` directory contains both the MNIST dataset. The grader should be able to run my homework scripts without altering this directory.

The `DML` directory contains all the auxiliary files used to do the computations in the homework scripts and has a logical hierarchy. For example, the directory `optimization` contains the file `gradient_descent.py` while contains both my batch gradient descent and stochastic gradient descent implementations. The directory `data_processing` contains the script `mnist_utils.py` which contains my functions used to load and work with the MNIST data. The directory `classification` contains the file `classifier_utils.py` which contains all things related to binary and softmax classification including the gradients for each respective method for use with a gradient descent algorithm. The `validation` sub-directory contains `validation.py`. This file contains all my loss functions such as 0/1 loss and also my implementations for regularization paths for both linear regression and logistic and softmax classification using gradient descent. Finally, the `regression` directory contains all utilities for a normal or multi-class regression. In each section, I try to be explicit with what files I used to perform the computation including the path from the `DML` directory for ease of grading.

QUESTION 0: COLLABORATORS

I collaborated with Matt Wilde, Serena Liu, and Janet Matsen for various questions on this assignment.

QUESTION 1: PCA AND RECONSTRUCTION

In this question, I derive matrix algebra relations and I use my PCA implementation to reduce the dimensionality of the MNIST dataset and visualize the results. The code used to solve this question is in the following attached files: `hw3_1.2.py`, `hw3_1.3.py`, `hw3_1.4.py` in the HW3 directory and `classification/classifier_utils.py`, `regression/regression_utils.py`, `validation/validation_utils.py`, `data_processing/mnist_utils.py`, `pca/pca.py` in the DML directory.

1.0: Details of my PCA implementation. My PCA implementation performs a SVD on the MNIST training data X to derive the principal components and the eigenvectors of the empirical covariance matrix, Eqn. 3. Performing PCA using a SVD gives me the following matrices: u , s , and v where the columns of v are the eigenvectors of Eqn. 3. The eigenvalues of Eqn. 3 are given by the square of the singular values divided by the length of the dataset, $\lambda = s^2/N$.

To transform the dataset to a lower dimensional space using the first l principal components, the first l columns of v , I evaluate

$$(1) \quad X_{trans} = Xv$$

since X is $N \times d$ and the truncated v is $d \times l$ resulting in a lower-dimensional $N \times l$ X_{trans} . I reproject my lower-dimensional transformed data back into “physical” space via

$$(2) \quad X_{approx} = X_{trans}v^T$$

since X_{trans} is $N \times l$ and v^T is $l \times d$ resulting in a $N \times d$ matrix. Note that $X_{approx} \neq X$ for $l < d$ principal components since using less than the total feature number of principal components instead yields an approximation of the original data when projected back into the original space.

Note that for all questions, I first centered the training data before running PCA. Specifically, for each feature (column) of X , I subtracted off its mean. In addition to the textbook suggesting this as a good practice, I found that it yielded better performance and hence do so for all PCA questions in this homework set in less explicitly stated otherwise.

1.1: Matrix Algebra Review. For this question, I will use the following definitions:

$$(3) \quad \Sigma = \frac{1}{N} \sum_i x_i x_i^T.$$

1.1.1. For brevity, I define $B^T = C$. First, I expand

$$\begin{aligned}
 (4) \quad \text{Tr}(AC) &= \sum_{i=1}^N (AC)_{ii} \\
 &= \sum_{i=1}^N \left(\sum_{k=1}^d A_{ik} C_{ki} \right) \\
 &= \sum_{i=1}^N \sum_{k=1}^d A_{ik} C_{ki}.
 \end{aligned}$$

Similarly, I expand

$$\begin{aligned}
 (5) \quad \text{Tr}(CA) &= \sum_{k=1}^d (CA)_{kk} \\
 &= \sum_{k=1}^d \left(\sum_{i=1}^N C_{ki} A_{ik} \right) \\
 &= \sum_{k=1}^d \sum_{i=1}^N C_{ki} A_{ik} \\
 &= \sum_{i=1}^N \sum_{k=1}^d A_{ik} C_{ki}
 \end{aligned}$$

which is equal to the above expression for $\text{Tr}(AC)$, completing the proof.

1.1.2. I will do this proof piece-wise. First, I note that $\Sigma = UDU^{-1}$ via a typical eigenvalue decomposition where D is the diagonal matrix with the eigenvalues of Σ along the d diagonals of D . Now,

$$\begin{aligned}
 (6) \quad \text{Tr}(\Sigma) &= \text{Tr}(UDU^{-1}) \\
 &= \text{Tr}(DU^{-1}U) \\
 &= \text{Tr}(D) \\
 &= \sum_{i=1}^d \lambda_i
 \end{aligned}$$

completing one equality using the relation derived in 1.1.1. Now for the last one, I expand Σ as

$$\begin{aligned}
 (7) \quad \Sigma &= X^T X \\
 &= [\vec{X}_1^T, \vec{X}_2^T, \dots, \vec{X}_n^T]^T \cdot [\vec{X}_1^T, \vec{X}_2^T, \dots, \vec{X}_n^T]
 \end{aligned}$$

which is a matrix with diagonals given by

$$\begin{aligned}
 & [\vec{X}_1 \cdot \vec{X}_1, \vec{X}_2 \cdot \vec{X}_2, \dots, \vec{X}_n \cdot \vec{X}_n] \\
 (8) \quad & = \sum_{i=1}^n (X^T X)_{ii}.
 \end{aligned}$$

Therefore,

$$\begin{aligned}
 Tr(\Sigma) &= \frac{1}{n} Tr(X^T X) \\
 (9) \quad &= \frac{1}{n} \sum_{i=1}^n (X^T X)_{ii} \\
 &= \frac{1}{n} \sum_{i=1}^n ||X_i||^2
 \end{aligned}$$

completing the proof.

1.2: PCA.

1.2.1. The eigenvalues $\lambda_1, \lambda_2, \lambda_{10}, \lambda_{30}, \lambda_{50}$ are 332719.1, 243279.9, 80808.5, 23685.7, and 11035.3, respectively. The sum of all eigenvalues is 3428445.4. Again, I calculate $\lambda = s^2/N$ for singular value s and dataset size N .

1.2.2. I plot the fractional reconstruction error for $k \in [1, 50]$ for the k principal components in Fig. 1. The fractional reconstruction error is defined as

$$(10) \quad F = 1 - \frac{\sum_{i=1}^k \lambda_i}{\sum_{i=1}^d \lambda_i}$$

for d total features and k principal components. Note how the first principal component is the largest eigenvalue as shown above.

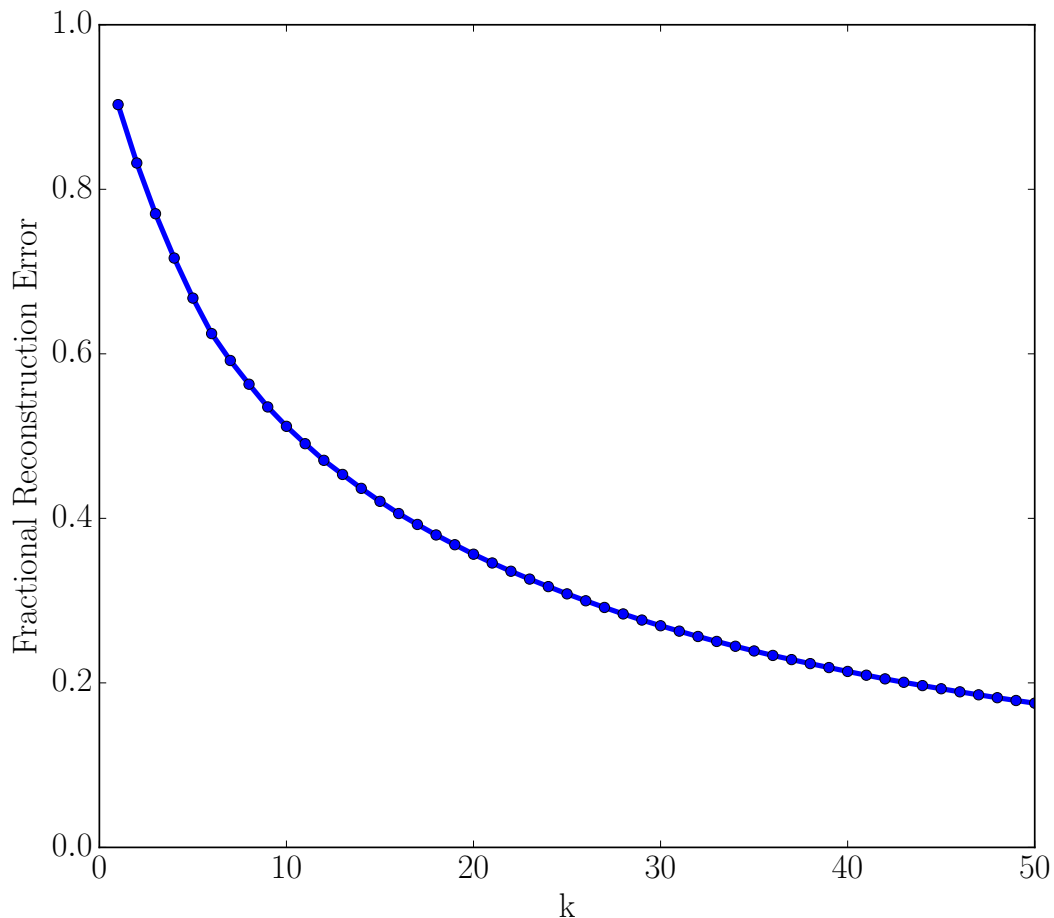


FIGURE 1. Fractional reconstruction error as a function of k principal components out of d total dimensions for $k \in [1, 50]$.

1.2.3. The first eigenvalue, and its corresponding principal component, represent the component of the data that captures the most variance. That is, the first eigenvalue represents the intensity dimensions. If the data is not centered, the first eigenvector captures the mean of the data.

1.2.4. I plot the fractional reconstruction error for $k \in [2, 50]$ for the k principal components in Fig. 2. As expected, we see that the absence of the first eigenvalue demonstrates its importance.

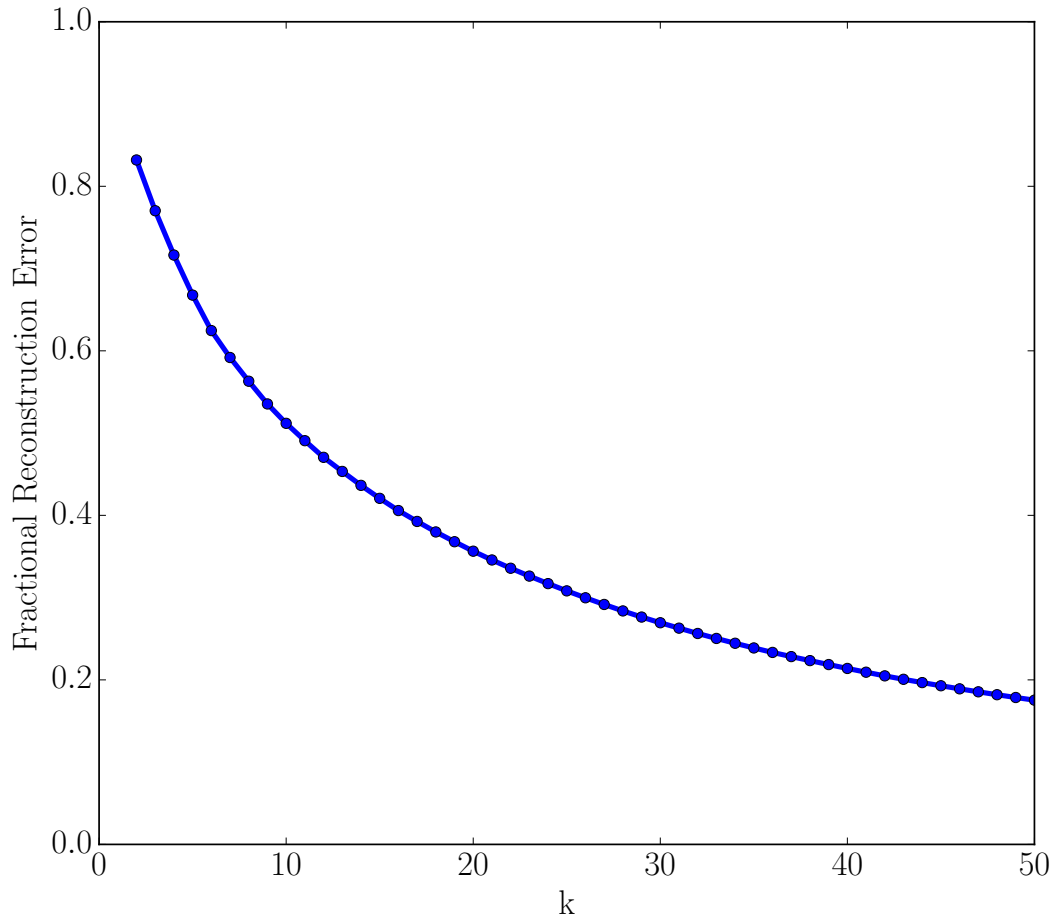


FIGURE 2. Fractional reconstruction error as a function of k principal components out of d total dimensions for $k \in [2, 50]$.

1.3: Visualization of the Eigen-Directions.

1.3.1. I plot the first 16 eigenvectors in Fig. 3 as images. To do so, I reshaped each vector into a 28×28 pixel image. For each image, I also annotate it with its number such that the second eigendirection would have a “2” in its image. I plotted 16 instead of 10 since 16 gives a nice symmetric collection of subplots.

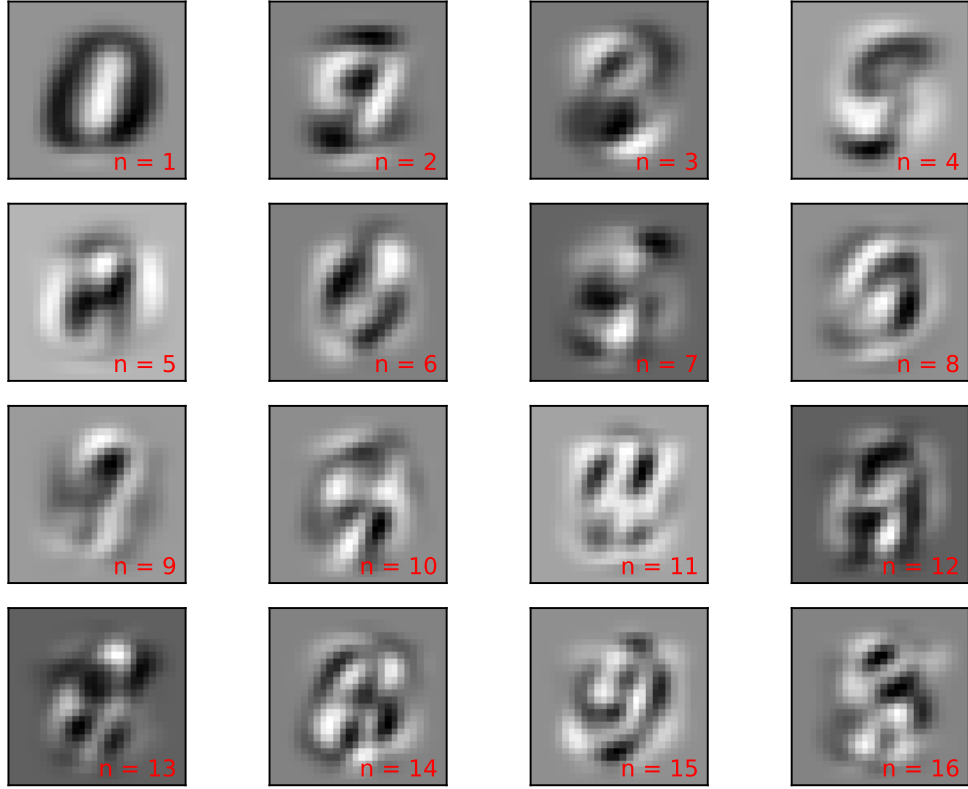


FIGURE 3. Visualization of the first 16 eigendirections as 28×28 pixel images. The respective eigendirection number is given in red in a subplot's lower righthand corner.

1.3.2. Each individual eigendirection, or principal component, captures a fundamental basis vector in an orthogonal set which each explain a decreasing variation in the data with increasing principal component number. That is, the first principal component accounts for the most variability in the data while subsequent components account for less and less variability. This intuitive picture makes sense upon examining Fig. 3. The first four components themselves appear to represent the numbers 0, 9, 3, and 5, respectively. Although the components are not actually those numbers, instead they capture characteristics of numbers in the dataset that are commonly shared. Many of the digits share features with 9, 3, and 5, for example, like their openings on the lefthand side of the digit and the solid vertical line on the righthand side of the digit.

1.4: Visualization and Reconstruction.

1.4.1. Here, I choose 6 unique digits from the MNIST training set and plot them in Fig. 4. I annotate each digit's image with its label in the lower-righthand corner. I chose 6 digits instead of 5 for symmetry's sake.

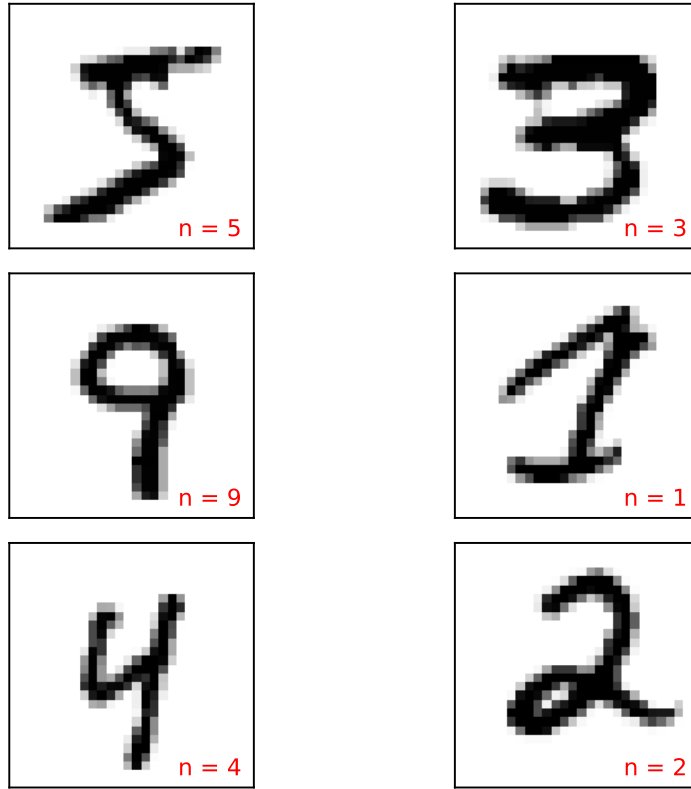


FIGURE 4. Visualization of 6 random, unique digits from the MNIST training set. The image label is displayed in red in the lower-righthand corner of each image.

1.4.2. Now I perform PCA on the MNIST training set keeping the first 100 principal components. Using this fit and the same digits displayed in Fig. 4, I reconstruct the digits using 2, 5, 10, 20, 50, and 100 principal components using the reconstruction $X_{recon} = Xvv^T$. The reconstructions are displayed in Fig. 5, Fig. 6, Fig. 7, Fig. 8, Fig. 9, and Fig. 10. For each reconstructed image using k principal components, k is shown in red in the lower-righthand corner.

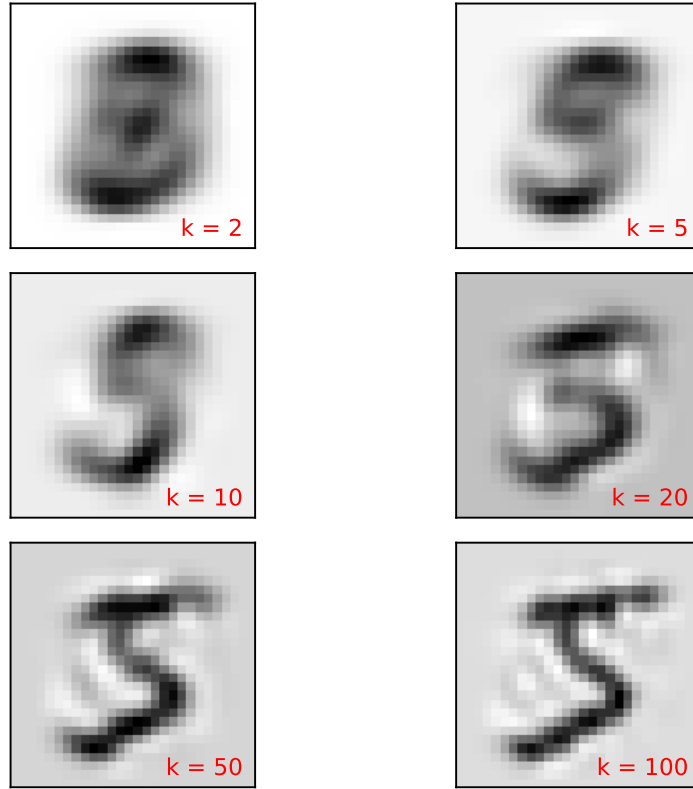
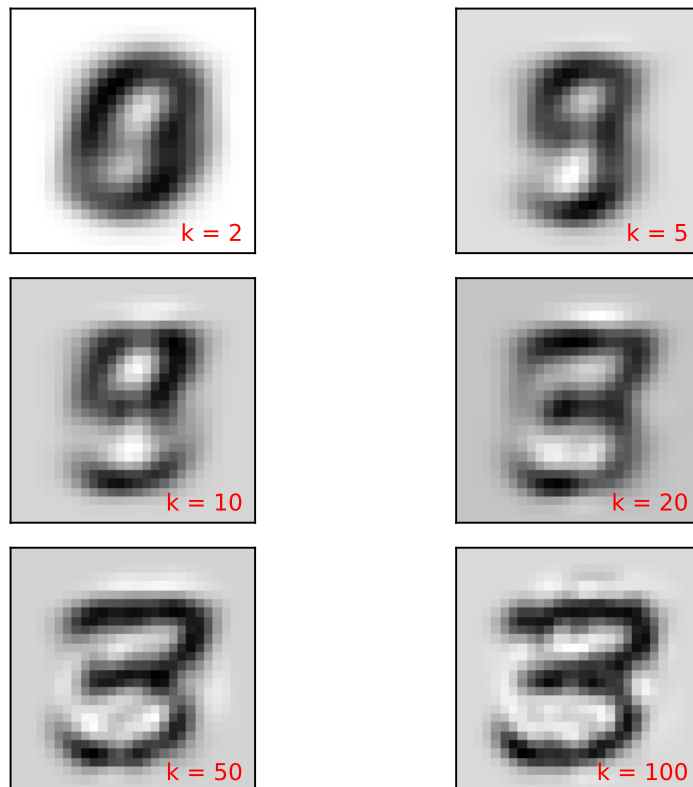


FIGURE 5. Reconstruction of a number 5 from the MNIST data set (see Fig. 4 using $k \in [2, 5, 10, 20, 50, 100]$ principal components where the given k is denoted in red in the lower-righthand corner of the respective subplot.



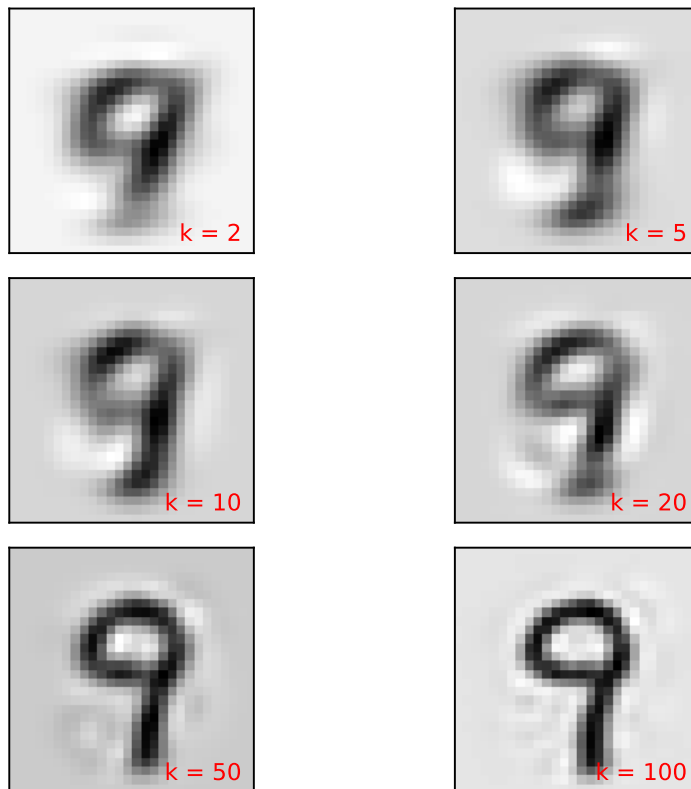


FIGURE 7. Reconstruction of a number 9 from the MNIST data set (see Fig. 4) using $k \in [2, 5, 10, 20, 50, 100]$ principal components where the given k is denoted in red in the lower-righthand corner of the respective subplot.

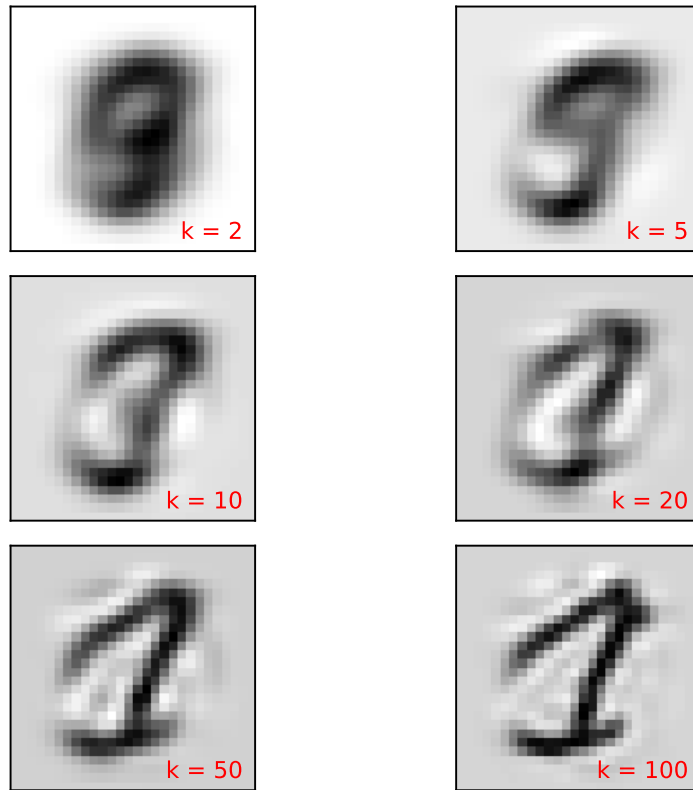


FIGURE 8. Reconstruction of a number 1 from the MNIST data set (see Fig. 4) using $k \in [2, 5, 10, 20, 50, 100]$ principal components where the given k is denoted in red in the lower-righthand corner of the respective subplot.

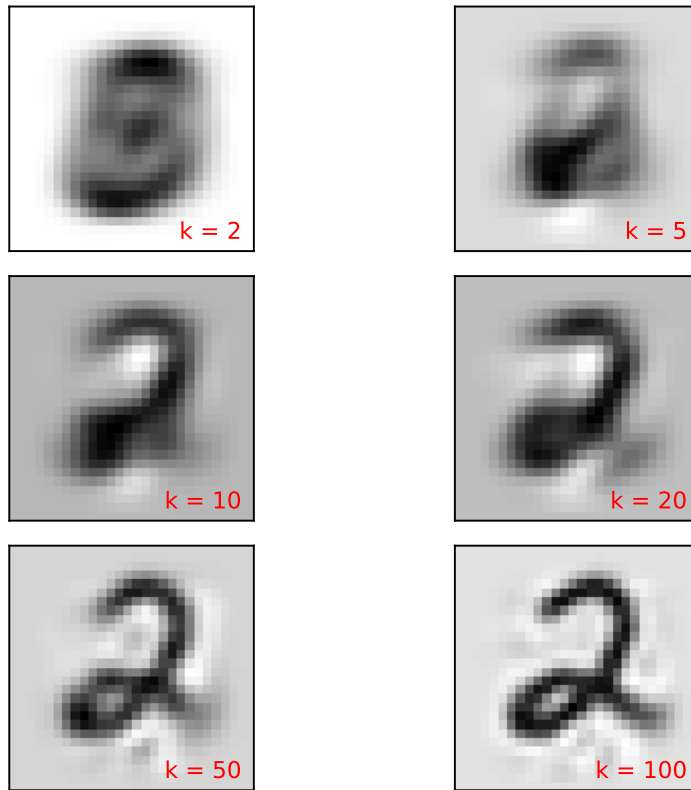


FIGURE 9. Reconstruction of a number 2 from the MNIST data set (see Fig. 4) using $k \in [2, 5, 10, 20, 50, 100]$ principal components where the given k is denoted in red in the lower-righthand corner of the respective subplot.

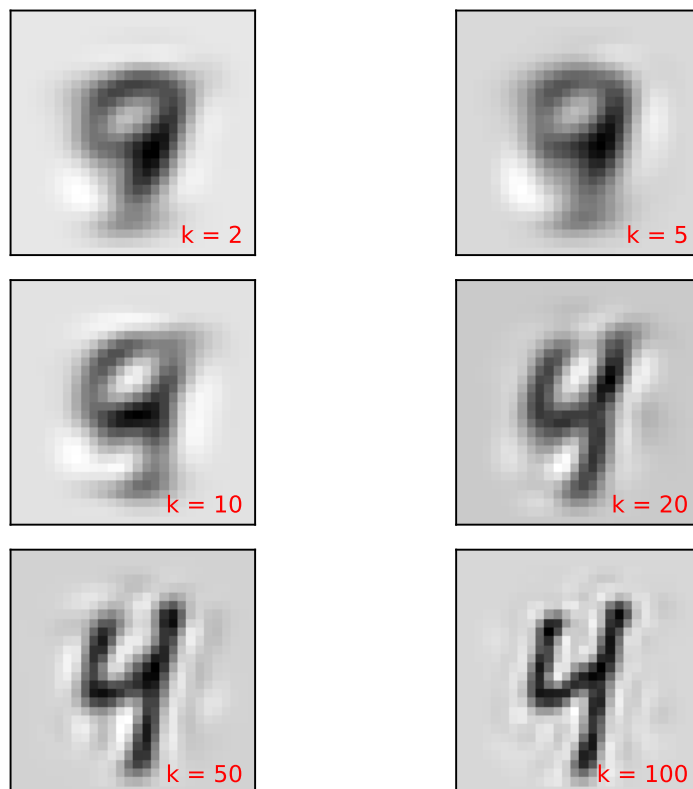


FIGURE 10. Reconstruction of a number 4 from the MNIST data set (see Fig. 4) using $k \in [2, 5, 10, 20, 50, 100]$ principal components where the given k is denoted in red in the lower-righthand corner of the respective subplot.

1.4.3. Broadly, the images reconstructed using at least $k = 20$ principal components appear to be a good, albeit grainy, approximation of the true image. Some images, in particular the reconstructed 9 and 5, are decently approximated using 10 principal components. Other digits that have large scatter in how they are drawn, such as 4s, require more principal components to adequately approximate the true image. All digits reconstructed with at least 50 principal components are good approximations of the original images. As expected, the more principal components used, the better the approximation becomes since as $k \rightarrow d$, we expect the reconstruction to become equal to the original X .

2: LET’S GET TO STATE OF THE ART OF MNIST!

In this section, I use one-against least-squares classification to attempt to get to “state of the art” on the MNIST dataset. The code used to solve this question is in

the following attached files: `hw3_2.py`, `hw3_2.2.py`, `hw3_2.3.py` in the HW3 directory and `pca/pca.py`, `regression/regression_utils.py`, `classification_utils.py`, `validation/validation.py`, `data_processing/mnist_utils.py`, `optimization/gradient_descent/kernel/kernel.py` all in the DML directory.

2.1 Least Squares. For computational speed purposes, I first performed dimension reduction using PCA. I fit my PCA algorithm on the MNIST training set with the mean subtracted out then projected each image using the first $k = 50$ components. I mapped the $n \times k$ reduced MNIST training data for n samples to a $n \times n$ transformed MNIST training set using a random Fourier feature approximation of an RBF kernel of the form

$$(11) \quad h_j(x) = \sin\left(\frac{v_i \cdot x}{\sigma}\right)$$

where $h_j(x)$ is the j th feature out of n of the transformed image x . The transformation matrix v is composed of $k = 60,000$ columns where each coordinate of the k columns are independently sampled from the standard normal distribution. The same matrix v was used to transform both the training and testing sets. I selected the bandwidth $\sigma = 780$ by taking the mean of the pairwise distance of about 100 samples and scaling that value by 3. I explored several other values for σ and found no improvement in performance.

Since the transformed training data matrix was so large, I used mini-batch SGD with a mini-batch size of 10 for all gradient calculations. Each epoch, or each complete pass through a randomly permuted training set, I performed $60,000/10 = 6,000$ mini-batch gradient updates. I computed the loss of the entire transformed training set and testing set (to which I applied the same transformation as the training set for consistency). In addition over a given epoch, I averaged the weight vectors and offset terms to get \bar{w} and \bar{w}_0 and used these to compute losses as well. I called my algorithm converged once the mean square loss on the training set did not change by more than 0.1%. I did not explicitly use regularization since the early-stopping from my learning rate decay scheme (described below) and my convergence criterion implicitly l_2 regularize my solution. I used this exact same optimization scheme for both Questions 2.2 and 2.3 (see below).

2.1.1. I used a learning rate $\eta = 3 \times 10^{-5}$ as gave the best fit. In practice in my SGD implementation at the start of each epoch, I reset $\eta = k\eta_0/N$ where N is the number of samples in a batch, $k = 1/\sqrt{t}$ is a scaling constant where t is the epoch number and $\eta_0 = 3 \times 10^{-5}$. I used a mini-batch size of 10 and a kernel bandwidth of 780 computed using the scheme described above.

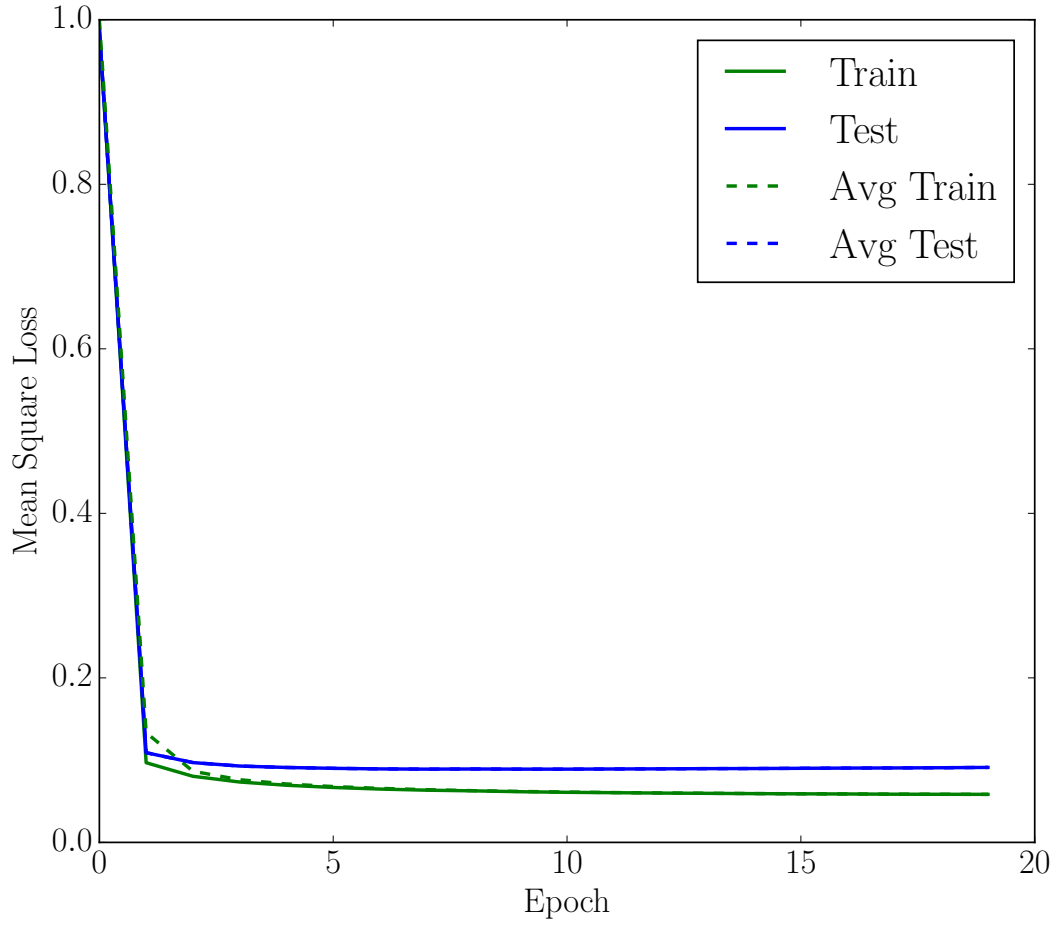


FIGURE 11. Mean square loss versus epoch for the both the MNIST training and testing sets for both the w_t (train, test) and \bar{w}_τ (avg train, avg test).

2.1.2. After the first iteration, both the training and testing losses drop dramatically and then slowly converge over the last iterations. Both the average training and test losses computing with the average weight vector over the epoch, \bar{w}_τ and \bar{w}_0 , perform slightly better than their unaveraged counterparts. As expected, the training loss is lower than the testing loss for all epochs.

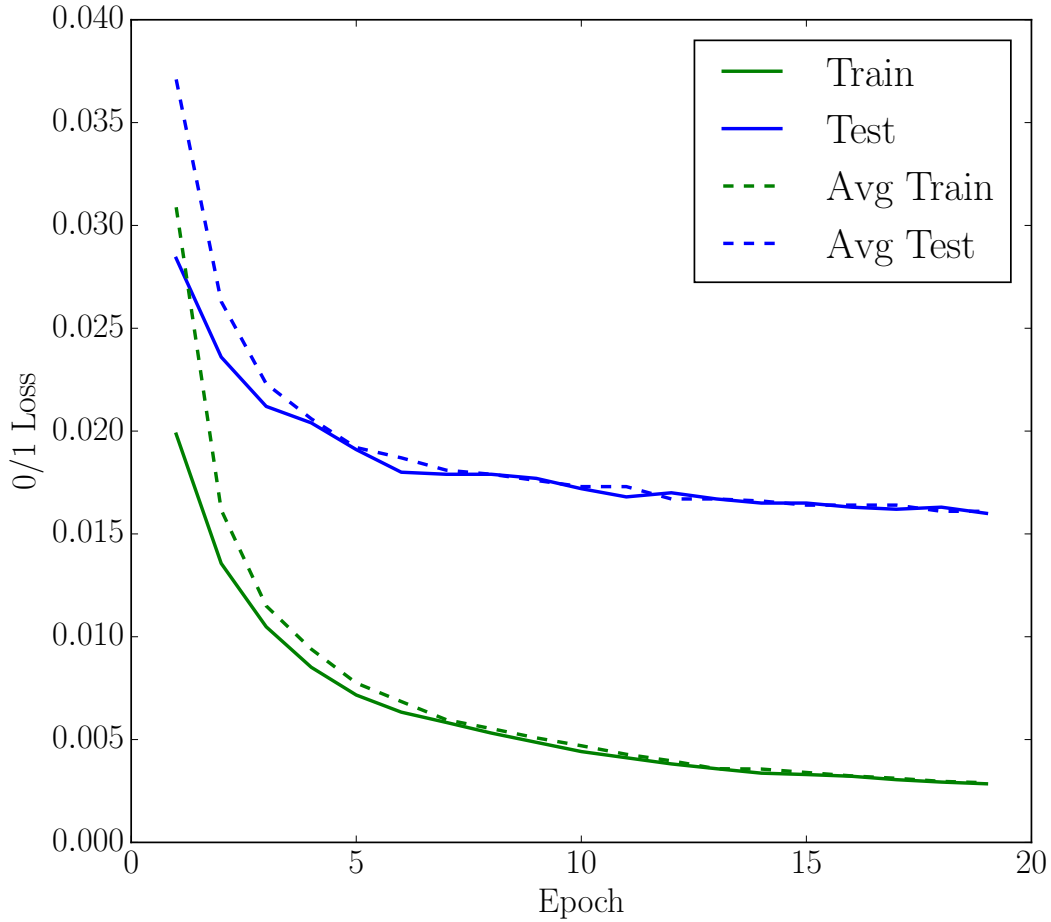


FIGURE 12. 0/1 loss versus epoch for the both the MNIST training and testing sets for both the w_t and \bar{w}_τ computed after the testing loss dipped below 5%.

2.1.3. As before, all 0/1 losses drop dramatically, well below 5%, after the first pass through the training set. From there on, they gradually converge with the testing loss ending up at about 1.6%. Interestingly, the averaged weight 0/1 losses for both the training and testing sets only start to perform as well as the un-averaged weight losses near the final iterations when the solution did not vary too much.

2.1.4. The final training squared loss and 0/1 loss are 0.0584 and 0.0029, respectively. The total number of mistakes made on the training set of the final point are

171. The same values computed using the weights averaged over the last epoch, \bar{w}_τ , are 0.0584, 0.0029, and 171, respectively.

2.1.5. The final testing squared loss and 0/1 loss are 0.0912 and 0.016, respectively. The total number of mistakes made on the testing set of the final point are 160. The same values computed using the weights averaged over the last epoch, \bar{w}_τ , are 0.0912, 0.0161, and 161, respectively.

2.2: EXTRA CREDIT: Softmax Classification. Here, I classify the PCA-reduced MNIST digits using the same transformation and procedure using in Question 2.1 except this time I optimize the log loss and classify using the soft max scheme as done in previous assignments.

2.2.1. I used a learning rate $\eta = 1 \times 10^{-4}$ as gave the best fit. In practice in my SGD implementation at the start of each epoch, I reset $\eta = k\eta_0/N$ where N is the number of samples in a batch, $k = 1/\sqrt{t}$ is a scaling constant where t is the epoch number and $\eta_0 = 1 \times 10^{-4}$. I used a mini-batch size of 100 and a kernel bandwidth of 780 computing using the scheme described above. In order to prevent my weights from becoming too large and causing the solution to diverge, I used a regularization constant of $\lambda = 1$. I empirically found that larger values yielded a worse solution and smaller values did not provide enough regularization to keep the solution stable. As before, I said my run was converged once the log loss stopped changing by more than 0.1%.

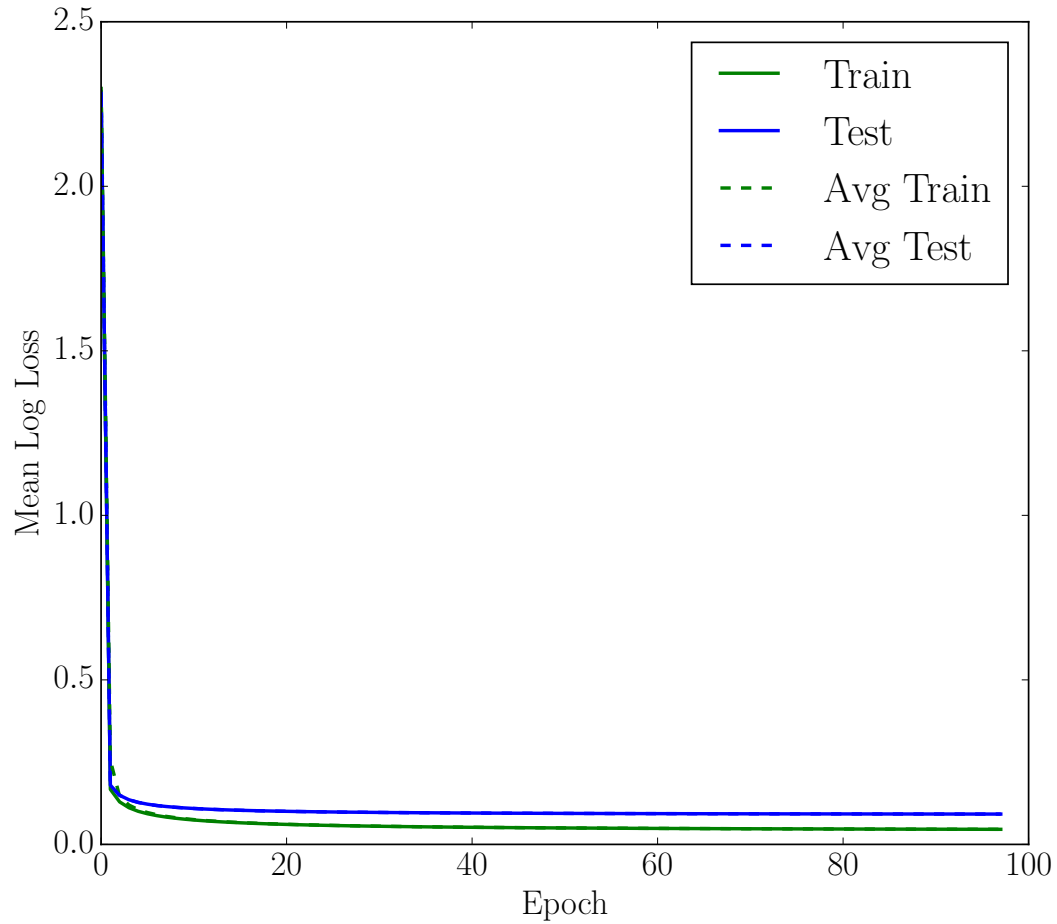


FIGURE 13. Mean log loss versus epoch for the both the MNIST training and testing sets for both the w_t and \bar{w}_τ .

2.2.2. Both the training and testing log loss drop rapidly on the first iteration and then slowly converges. As expected, the training log loss was appreciably lower than the testing log loss. There was no significant difference between the losses computing using w_t and \bar{w}_τ .

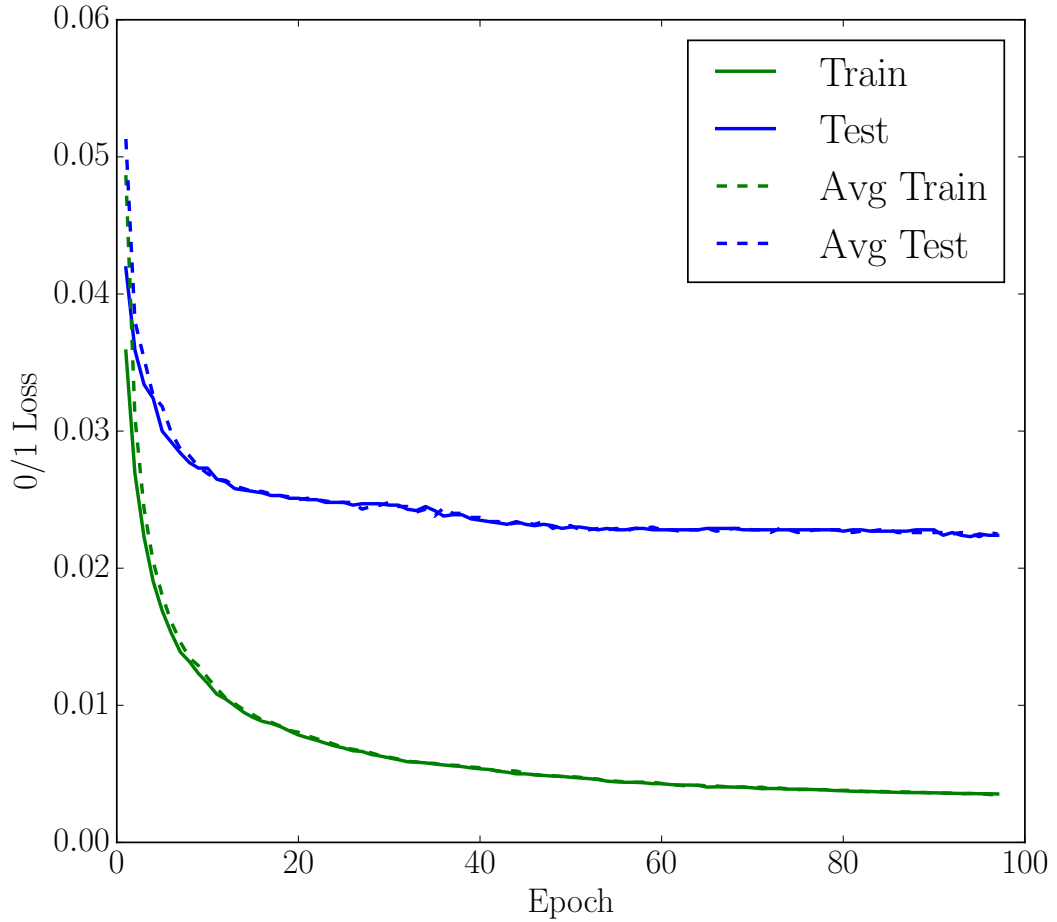


FIGURE 14. 0/1 loss versus epoch for the both the MNIST training and testing sets for both the w_t and \bar{w}_τ computed after the testing loss dipped below 5%.

2.2.3. Both the training and testing 0/1 losses dropped dramatically during the first iteration with the testing loss being noticeably worse than the training loss, as expected. Although it appears as if the training 0/1 loss could still decrease, the testing 0/1 loss curve had effectively flatten out suggesting that any further gradient steps would lead to overfitting and potentially worse testing set performance. At later epochs, there was no appreciable difference between 0/1 losses computed with w_t and \bar{w}_τ .

2.2.4. The final training log loss and 0/1 loss are 0.0458 and 0.0035, respectively. The total number of mistakes made on the training set of the final point are 212. The same values computed using \bar{w}_τ are 0.0458, 0.0035, and 212, respectively.

2.2.5. The final testing log loss and 0/1 loss are 0.0922 and 0.0224, respectively. The total number of mistakes made on the testing set of the final point are 224. The same values computed using \bar{w}_τ are 0.0922, 0.0225, and 225, respectively. This classifier does not perform as well as the Fourier feature case in Question 2.1, but it still performs rather well.

2.3: EXTRA CREDIT: Back to those random Neural Net Features.

For this question, I instead mapped the PCA-reduced image using the neural net features computed using the same outline given in previous homework:

$$(12) \quad h_j(x) = \max(v \cdot x, 0)$$

where there are $k = 60,000$ h_j in each transformed image. I optimized my solution using the square loss and classified using an ordinary least square “one-against-all” classifier for 10 classes.

2.3.1. I used a learning rate $\eta = 3 \times 10^{-11}$ as gave the best fit. In practice in my SGD implementation at the start of each epoch, I reset $\eta = k\eta_0/N$ where N is the number of samples in a batch, $k = 1/\sqrt{t}$ is a scaling constant where t is the epoch number and $\eta_0 = 3 \times 10^{-11}$. I used a mini-batch size of 10 and a kernel bandwidth of 780 computing using the scheme described above. As before, I deemed my solution converged once the loss stopped changing by more than 0.1%.

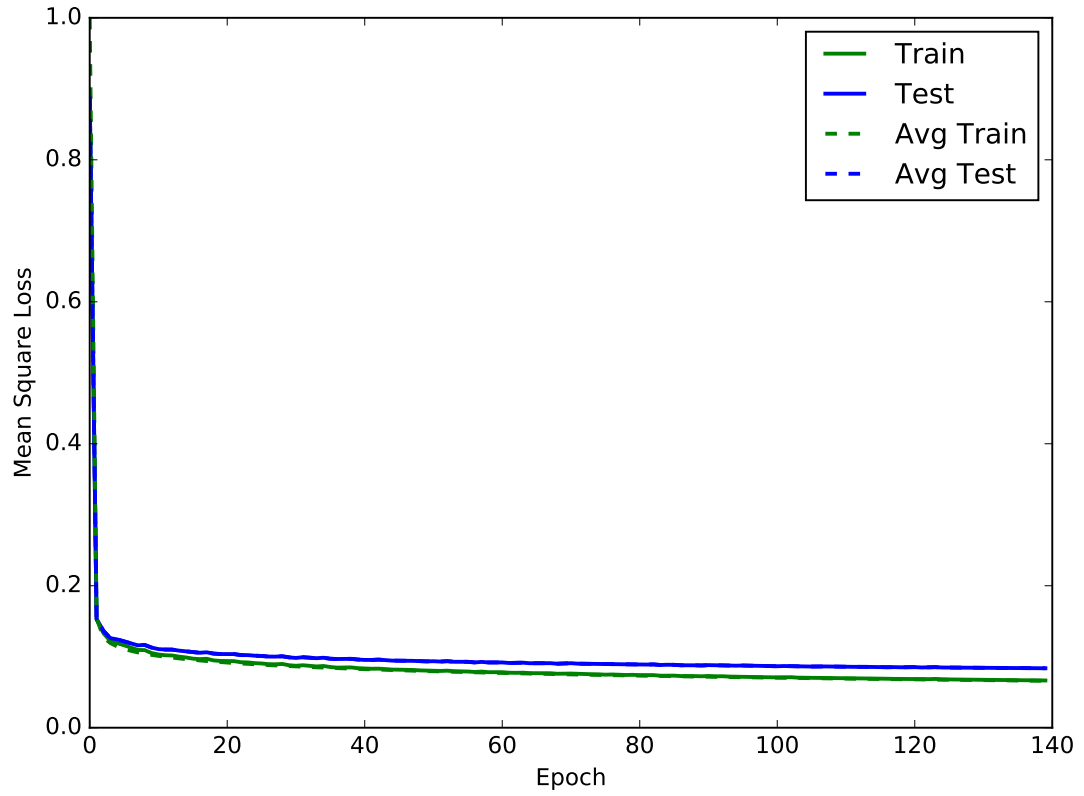


FIGURE 15. Mean square loss versus epoch for the both the MNIST training and testing sets for both the w_t and \bar{w}_τ .

2.3.2. As shown before, the square loss rapidly drops on the first iteration and then converges slowly for both the training and testing set. At later epochs, no appreciable difference is seen between losses computed using w_t and \bar{w}_τ . As expected, the training loss is less than the testing set loss.

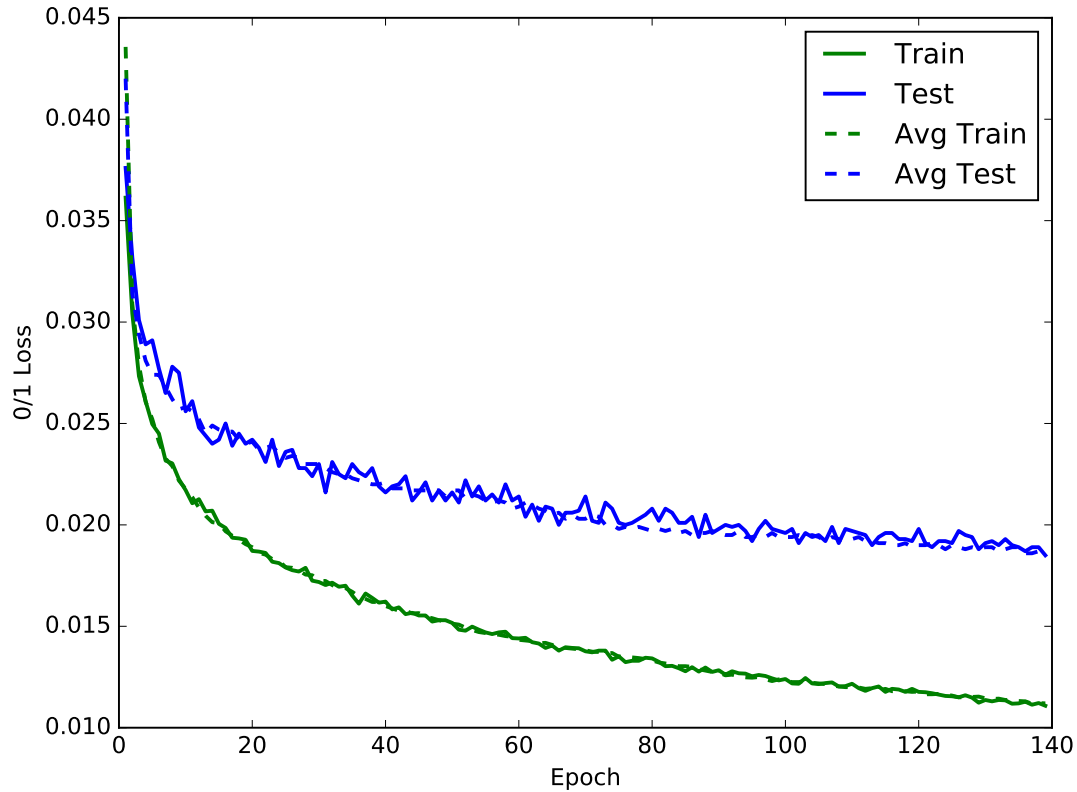


FIGURE 16. 0/1 loss versus epoch for the both the MNIST training and testing sets for both the w_t and \bar{w}_τ computed after the testing loss dipped below 5%.

2.3.3. Both the training set and testing set 0/1 loss drops rapidly in the first few iterations and continues to drop. Even though this optimization ran for many epochs and was deemed converged, it appears as if both the training and testing 0/1 loss would continue to decrease with additional epochs. Computational time constraints prevented the continued optimization of this problem. One interesting feature not observed in the optimization over the Fourier feature transformed datasets is the scatter in the 0/1 loss, especially for the testing loss. The 0/1 loss curves for the Fourier features were much smoother and appeared to monotonically decrease with epoch as opposed to the more noisy solution observed here. In cases like this, it is obvious why averaging the weight vector is useful. Not only would it beat down the noisy solution, it can also lead to better performance.

2.3.4. The final training square loss and 0/1 loss are 0.0665 and 0.0111, respectively. The total number of mistakes made on the training set of the final point are 665. The same values computed using \bar{w}_τ are 0.0661, 0.0112, and 672, respectively.

2.3.5. The final testing square loss and 0/1 loss are 0.0837 and 0.0185, respectively. The total number of mistakes made on the testing set of the final point are 185. The same values computed using \bar{w}_T are 0.0837, 0.0187, and 187, respectively. This classifier does not perform as well as the Fourier feature case in Question 2.1, but it still performs rather well.

3: SVMs: HINGE LOSS AND MISTAKE BOUNDS

Here, I work with a SVM which classifies according to the hypothesis:

$$(13) \quad h_w(x) = \text{sgn}(w^T x)$$

and the SVM loss function, the hinge loss, is given by

$$(14) \quad l((x, y), w) = \max(0, 1 - yw^T x)$$

for $y \in [-1, 1]$.

3.1. I can show that a function is convex if it is lower-bounded by its gradient (or subgradient, more generally). Here, I will examine the $y = 1$ case since the $y = -1$ case proceeds analogously. For the $w^T x > 1$ case, Eqn. 14 gives 0. The gradient with respect to w in this regime is 0 and lower-bounds then function. When $w^T x < 1, w^T x \neq 0$, the gradient with respect to w in this regime is $-X$. Since this is linear and $w^T X$ is linear with w , its gradient lower bounds it. Finally when $w^T x = 1$, the hinge point, the derivative is undefined so instead I use a subgradient. For the subgradient, it can be anything tangent line with slope between $[-X, 0]$, so I will use 0 for simplicity. This too lower bounds the function. Since the function is lower-bounded by its (sub)gradient at all points, it is convex. A similar argument applies for the $y = -1$ case.

3.2. For a correct prediction, $y_i = \text{sgn}(w^T x_i)$ holds. Here, I will just consider the $y = 1$ case for simplicity since the $y = -1$ case proceeds analogously. Here, the hinge loss is given as $HL = \max(0, 1 - w^T X)$. Since $w^T X < 0$ cannot occur when $y_i = 1 = \text{sgn}(w^T x_i)$, I will not consider it. If $w^T X = 0$, then the hinge loss is 1. If $w^T X \geq 1$, the hinge loss is 0. Therefore for correct predictions, the hinge loss ranges from $HL \in [0, 1]$.

3.3. Define the mistake bound as

$$(15) \quad \frac{1}{n} M(w) \leq \frac{1}{n} \sum_{i=1}^n \max(0, 1 - y_i w^T x_i)$$

where in my proof I will ignore the $1/n$ factor since it is merely a normalization term. If you consider the two regimes where your predictions are incorrect and correct, Eqn. 15 becomes

$$(16) \quad M(w) \leq \sum_{w^T x_i \in \text{correct}} \max(0, 1 - y_i w^T x_i) + \sum_{w^T x_i \in \text{incorrect}} \max(0, 1 - y_i w^T x_i).$$

The sum over the correct predictions will always be ≥ 0 since in the above question I showed that the hinge loss ranges from $[0, 1]$ for correct predictions. The sum over incorrect predictions will be at least to $M(w)$ since for the hinge loss for an incorrect prediction, the best you can do is 1 when $w^T x = 0$. Therefore if all your all your incorrect predictions are these “best” incorrect predictions, the sum over all incorrect predictions will be $M(w)$, giving you the stated lower bound and proving Eqn. 15.

4: FITTING AN SVM CLASSIFIER BY HAND

The code used for this question is given in `hw3.4.py` in the DML directory. For this section, I applied the $\phi(x) = (1, \sqrt{2}x, x^2)^T$ transformation to the two one dimensional samples.

4.1. Since the optimal vector \hat{w} is perpendicular to the decision boundary, I need to find a vector parallel to any line which is perpendicular to the decision boundary. Here I only deal with two points, so the decision boundary is readily identified as the plane going through the midpoint between the two points. A vector pointing to the midpoint of the two points will then be perpendicular to the decision boundary and parallel to \hat{w} . I can calculate that point as

$$\begin{aligned}
 (17) \quad & (\vec{\phi}(x_2) - \vec{\phi}(x_1))/2 \\
 & = ((1, 2, 2) - (1, 0, 0))/2 \\
 & = (0, 1, 1) = w.
 \end{aligned}$$

4.2. The margin is the distance from one point to the decision boundary. Since the decision boundary is the midpoint between the two points, the margin will be half the distance between the two points and is given by

$$(18) \quad \gamma = \frac{1}{2} \sqrt{(1-1)^2 + (2-0)^2 + (2-0)^2} = \sqrt{8}/2 = \sqrt{2}.$$

4.3. Given that the margin is given by $\gamma = 1/||w||$ and that \hat{w} is parallel to w by design, I can solve for \hat{w} as follows

$$\begin{aligned}
 (19) \quad & \gamma = 1/||w|| \\
 & 1/\sqrt{2} = \sqrt{2c^2} \\
 & 1/2 = 2c^2 \\
 & 1/4 = c^2 \\
 & 1/2 = c
 \end{aligned}$$

where $\hat{w} = (0, c, c) = (0, 1/2, 1/2)$.

4.4. I compress the tight inequality into an equality to satisfy equations 1-3. Inserting \hat{w} into equation 2 gives

$$\begin{aligned}
 (20) \quad & y_1(w^T \phi(x_1) + w_0) = 1 \\
 & - 1((0, 1/2, 1/2) \cdot (1, 0, 0) + w_0) = 1 \\
 & - w_0 = 1 \\
 & w_0 = -1
 \end{aligned}$$

and similarly equation 3 becomes

$$\begin{aligned}
 (21) \quad & y_2(w^T \phi(x_2) + w_0) = 1 \\
 & 1((0, 1/2, 1/2) \cdot (1, 2, 2) + w_0) = 1 \\
 & 1 + 1 + w_0 = 1 \\
 & w_0 = -1.
 \end{aligned}$$

Therefore, $w_0 = -1$.

4.5. If $f(x) = w_0 + \hat{w}^T \phi(x)$, I can write

$$(22) \quad f(x) = \frac{1}{2}x^2 + \frac{\sqrt{2}}{2}x - 1.$$

I plot Eqn. 22 and the two points \vec{x}_1 and \vec{x}_2 in Fig. 17.

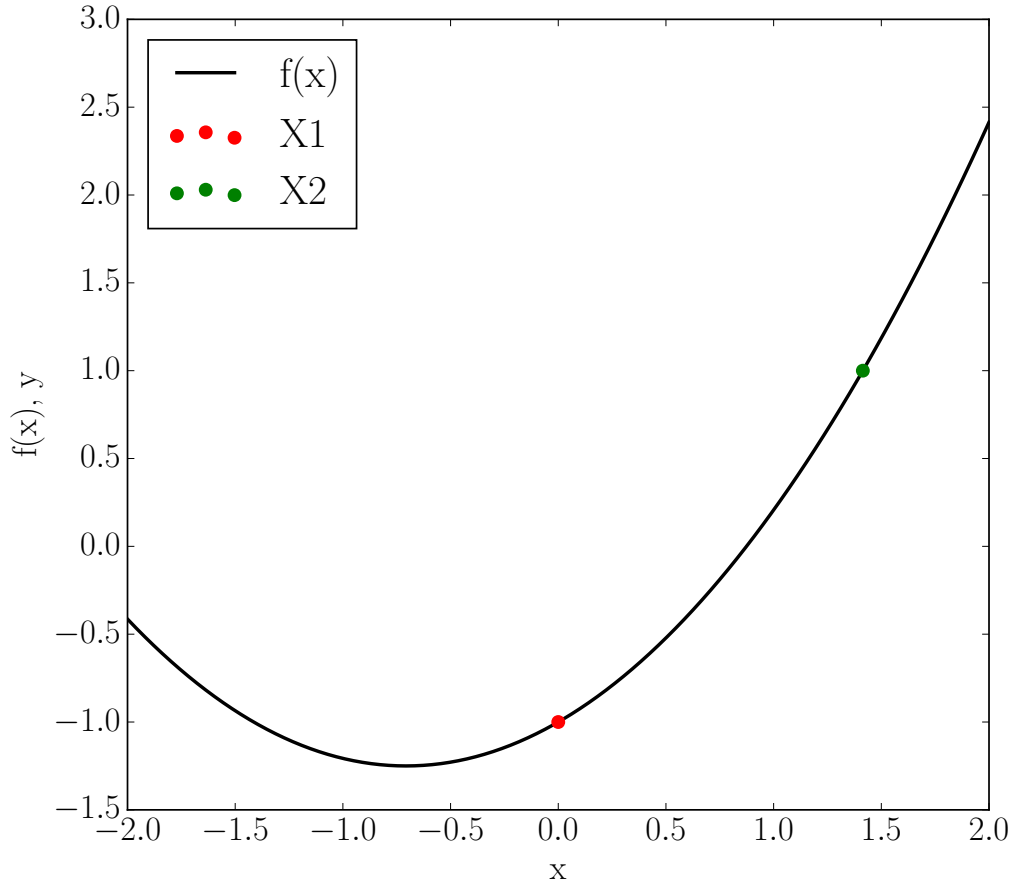


FIGURE 17. A plot of $f(x)$ and \vec{x}_1 and \vec{x}_2 projected into 2D space.

5: K-MEANS

In this question, I implement the K-means clustering algorithm and apply it to the MNIST dataset. The code used to solve this question is in the following attached files: `hw3_5.1.py`, `hw3_5.2.py` in the HW3 directory and `clustering/kmeans.py`, `validation/validation.py`, `data_processing/mnist_utils.py` in the DML directory.

5.0: K-Means Algorithm Implementation. My K-means algorithm follows the algorithm presented in the Murphy textbook. First, I initialize my k clusters using k random samples from the MNIST training set to make a $k \times d$ cluster matrix μ for d features. Each iteration, I perform the following E and M steps. In

the E step, I assign a label z to each sample X_i subject to

$$(23) \quad z_i = \operatorname{argmin}_k \|X_i - \mu_k\|_2^2$$

which assigns a point X_i to the closest cluster center μ_k according to the squared Euclidean distance. After passing through the training set and assigning each point to its nearest cluster center, I perform the M step in which I calculate the new cluster centers to be the centroids of the samples in each cluster as follows

$$(24) \quad \mu_k = \frac{1}{N_k} \sum_{i=1}^{N_k} X_i$$

where there are N_k samples in the k th cluster. I call the algorithm converged once all the samples' labels no longer change.

5.1: Run the algorithm. I ran the K-means algorithm with $k = 16$ on the full MNIST training set. As stated above, I initialized my centers μ_k using k random samples from the training set.

5.1.1a. In Fig. 18, I plot the squared reconstruction error versus iteration number for $k = 16$ clusters. I compute the squared reconstruction error as

$$(25) \quad \text{SRE} = \frac{1}{N} \sum_{j=1}^k \sum_{X_i \in \mu_j} \|X_i - \mu_j\|_2^2$$

where μ_j is the cluster X_i belongs to.

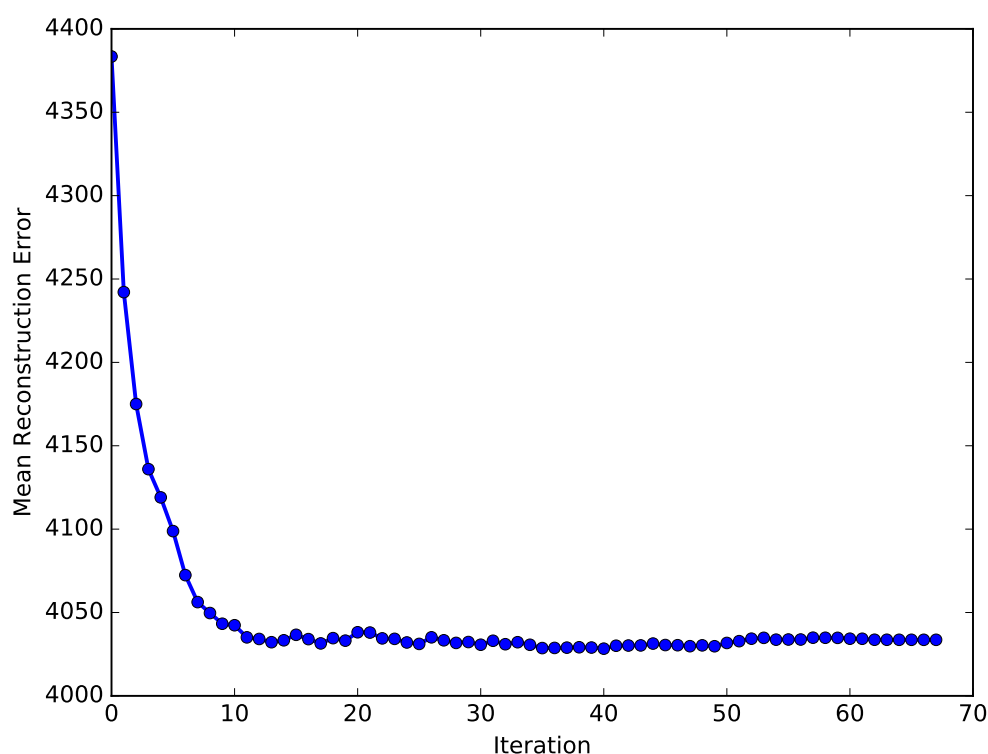


FIGURE 18. Squared reconstruction error versus iteration number for $k = 16$ clusters.

The mean squared reconstruction error reaches near its local minimum after about 10 iterations and does not change significantly over the next 60 iterations it takes the algorithm to converge. The final 60 or so iterations likely involved just a few points flipping labels, explaining why the error did not change appreciably.

5.1.1b. Let us define the number of assignments for a mean to be the number of samples assigned to that mean's cluster. In Fig. 19, I plot the number of assignments per cluster for $k = 16$ clusters ordered in descending order.

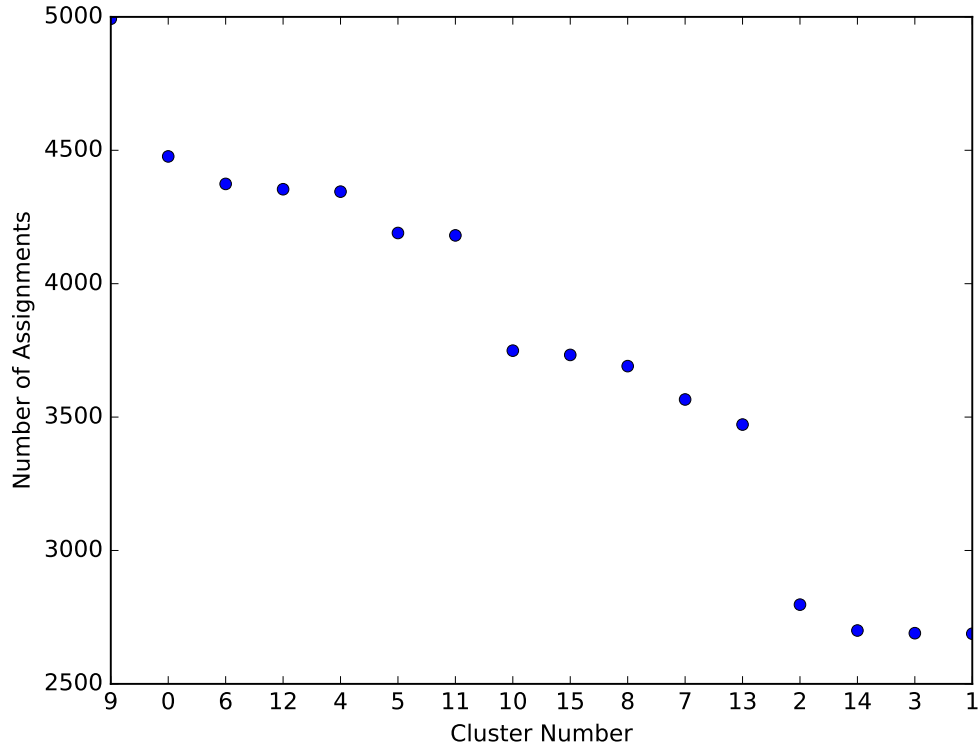


FIGURE 19. Number of assignments per cluster for $k = 16$ clusters ordered in descending order.

As can be seen in the above figure, cluster 9 contains the most members at about 5,000 while cluster 1 contains the least with around 2,700 members. I note that cluster number does not in general equal the MNIST digit label.

5.1.1c. In Fig. 20, I visualize the $k = 16$ centers my K-means algorithm learned on the MNIST training set in descending order for number of assignments.

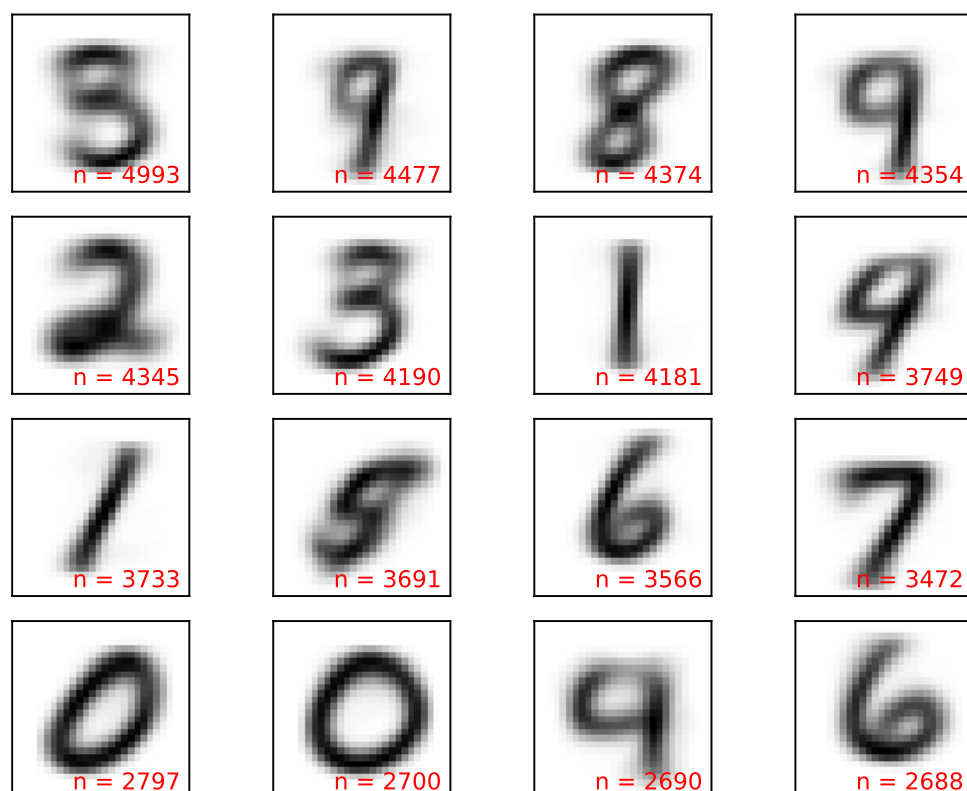


FIGURE 20. Visualization of the $k = 16$ centers orders by number of members. The number of members for each center is shown in each respective center's subplot in red in the lower-righthand corner.

5.1.2. For my $k = 16$ cluster visualization, I find it interesting that there appears to be two classes of clusters: some that are different rotations or transformations of a given digit or some that are amalgamations of similar digits. For example, there are several “6”s in the clusters that are rotations or transformations of a 6, and similarly for 1s and 0s. On the other hand, some cluster centers look like combinations of digits, such as combinations of 3s and 5s and combinations of 4s and 9s. These behaviors make sense because of the inherent variance in how people write digits. Not all digits are written in the same orientation or with the same curvature at certain parts of the digit causing some to look like others.

5.1.2a. I ran the K-means algorithm with $k = 250$ on the full MNIST training set. As stated above, I initialized my centers μ_k using k random samples from the training set. In Fig. 21, I plot the squared reconstruction error versus iteration number for $k = 250$ clusters. I compute the squared reconstruction error as in Eqn. 25.

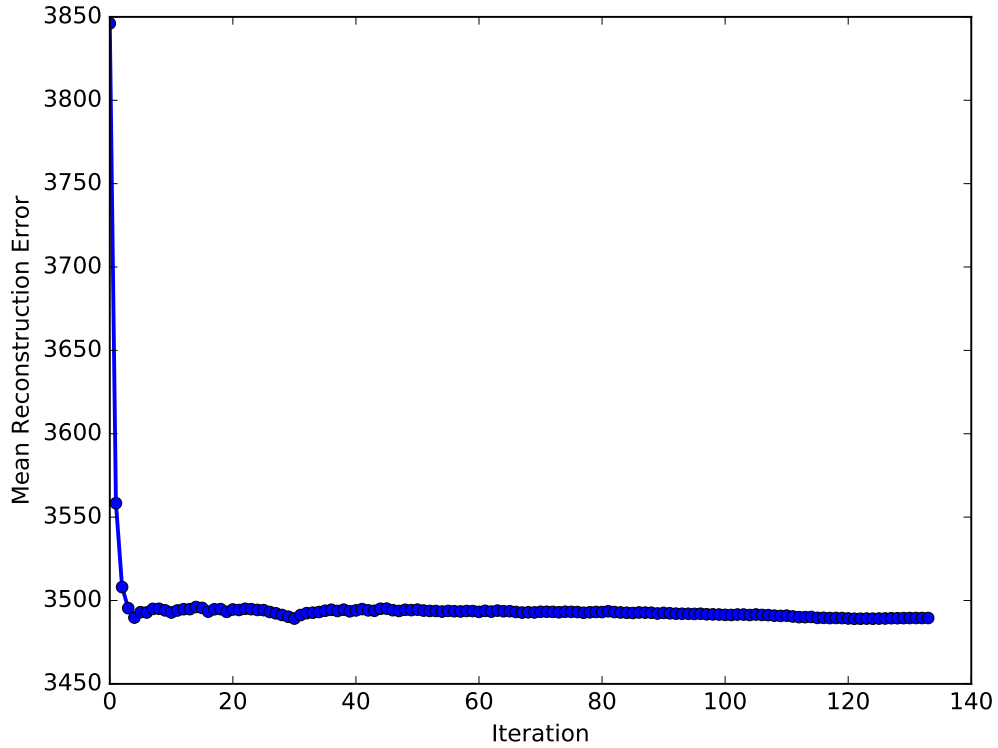


FIGURE 21. Squared reconstruction error versus iteration number for $k = 250$ clusters.

The mean squared reconstruction error reaches near its local minimum after about 5 iterations and does not change significantly over the next 125 iterations it takes the algorithm to converge. The final 125 or so iterations likely involved just a few points flipping labels, explaining why the error did not change appreciably and slowly decreased.

5.1.2b. In Fig. 22, I plot the number of assignments per cluster for $k = 250$ clusters ordered in descending order.

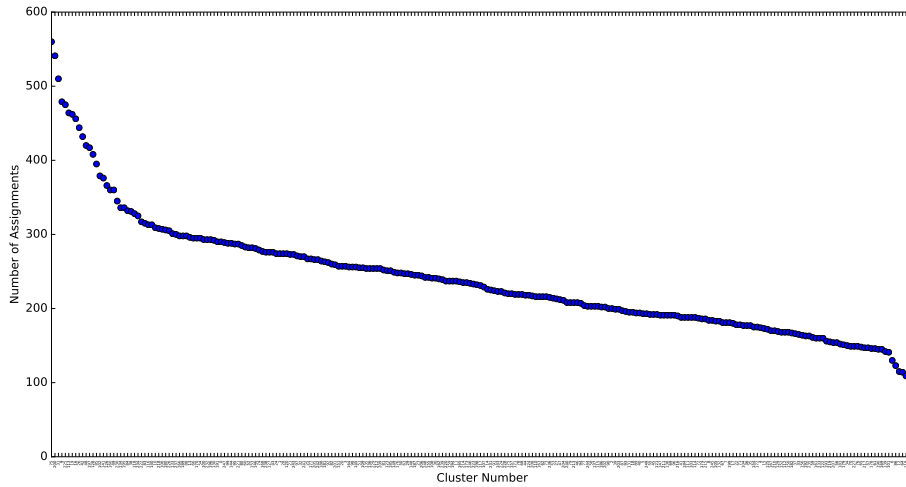


FIGURE 22. Number of assignments per cluster for $k = 250$ clusters ordered in descending order.

Interestingly, there appears to be 3 regimes that each cluster center falls into. The first regime involves the first 30 centers or so in which the number of assignments rapidly drops off, indicating that perhaps a smaller number of cluster centers really matter in terms of clustering, perhaps analogous to how PCA picks out the most important “directions” in a dataset. The next regime is a smooth, linear decrease in assignments due to clusters have less and less importance. The final regime is a steep decrease in assignments and corresponds to the least important clusters.

5.1.2c. In Fig. 23, I visualize the top 16 from my $k = 250$ centers my K-means algorithm learned on the MNIST training set in descending order for number of assignments.

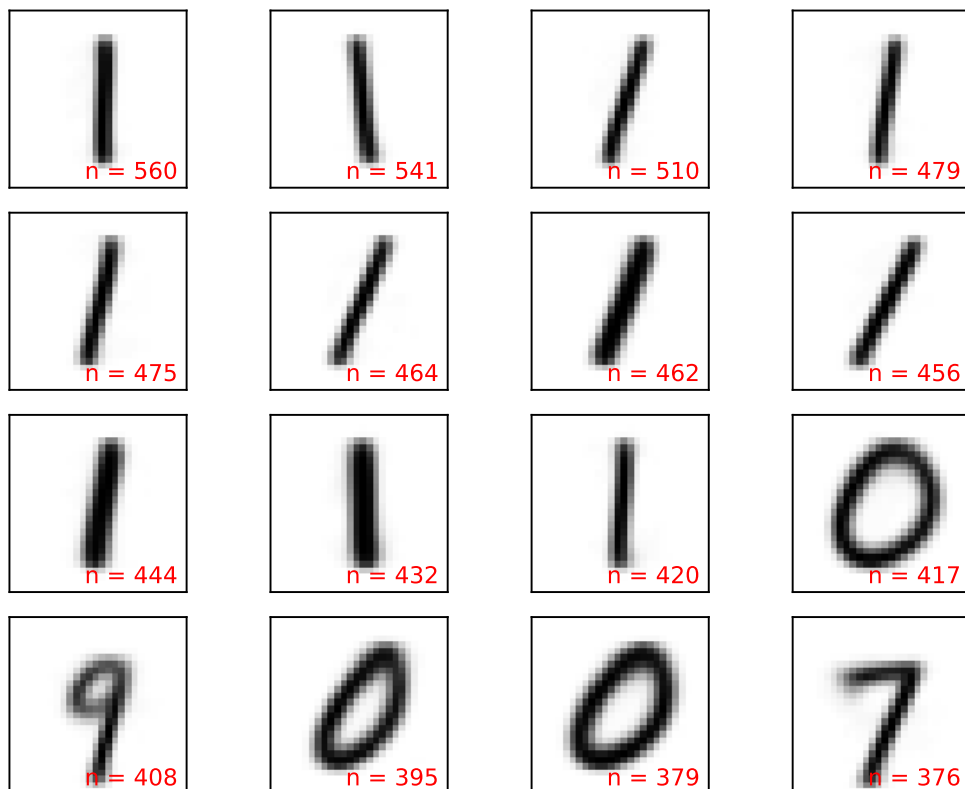


FIGURE 23. Visualization of the $k = 250$ centers orders by number of members. The number of members for each center is shown in each respective center's subplot in red in the lower-righthand corner.

From the figure it appears that the algorithm picked out various representations of a “1” as some of the most important cluster centers! What I believe is going on is that a dominant feature in the MNIST digits is the right hand side of the digits. Digits like 1, 3, 4, 5, 7, and 9 all have a more or less linear right hand side that, depending on who writes it, can slant in various orientations. What this learning procedure did is identify, more or less, how certain digits tended to slope in some ways. For example, one of the “1”s is sloped in such a way that it looks like the base of a 7, so perhaps many 7s were attributed to that cluster.

5.2: Classification with K-means. In this section I used my $k = 16$ and $k = 250$ K-means algorithms learned on the entire MNIST training set to classify digits. I classified a digit by finding a label for each center based on the most frequent digit assigned to it. For each sample, I found its closest center according to the squared Euclidean distance and used the label for that center.

5.2.1. My $k = 16$ cluster K-means fit achieved 0/1 loss of 0.333 and 0.327 on the training and testing sets, respectfully. Interestingly, the testing error was lower than the training error but I note that there was appreciable scatter between 0/1 losses for different fits using $k = 16$ on the training set and both 0/1 losses were quite high.

5.2.2. My $k = 250$ cluster K-means fit achieved 0/1 loss of 0.089 and 0.084 on the training and testing sets, respectfully. Interestingly, the testing error was lower than the training error but I note that there was appreciable scatter between 0/1 losses for different fits using $k = 250$ on the training set. The 0/1 loss in this case is roughly a factor of 3 lower than for the $k = 16$ case. This likely occurred because the additional clusters can help distinguish between differently drawn digits of the same class, such as 4s written differently by different people.